

Factors affecting the strength of P{011}<566>-texture after annealing of a cold-rolled Al–Mn–Fe–Si alloy

K. Huang^{1,2} · Y. J. Li¹ · K. Marthinsen¹

Received: 2 December 2014 / Accepted: 27 April 2015 / Published online: 5 May 2015
© Springer Science+Business Media New York 2015

Abstract Elongated coarse P{011}<566>-oriented grains are frequently observed after annealing of cold-rolled Al–Mn alloys with a highly supersaturated solid solution level. In this study, important factors affecting the strength of the P-texture component after annealing of a cold-rolled Al–Mn–Fe–Si alloy have been systematically investigated and their influence has been documented. The strength of the P-texture component has been analysed in terms of orientation distribution functions, area fractions and number fractions of P-grains at different conditions using EBSD. The strength of the P-texture is very sensitive to the micro-chemistry state in terms of the amount of Mn in solid solution (potential for concurrent precipitation) and pre-existing second-phase particles (dispersoids). In conditions of a significant P-texture, decreasing annealing temperature and heating rate, as well as increasing the amount of deformation before annealing, promotes a strengthening of the P-texture component. Detailed analyses clearly show that the strong P-texture is either due to a growth advantage of P-oriented grains at lower annealing temperatures or due to their dominating number fraction at higher temperatures. The

differences in terms of P-texture intensity are explained in view of the influence of second-phase particles (dispersoids) on the recrystallization nucleation and growth behaviour.

Introduction

Recrystallization textures, formed when deformed metals are annealed, have long been a subject of extensive investigation. The reason is partly their technological significance, i.e. these textures are the main factor responsible for the possible anisotropy of mechanical properties of semi-finished products. Moreover, since their origin and evolution are still not fully understood, recrystallization textures are also of great scientific interest. The recrystallization texture of cold-rolled high-purity aluminium alloys is often characterized by the cube orientation which is generally strengthened in intensity by high rolling reductions and high annealing temperatures [1]. However, almost all commercial aluminium alloys contain second-phase particles formed either before or during the recrystallization annealing. During the solidification of Al–Mn–Fe–Si (AA3xxx) alloys, most of the Fe content forms intermetallic constituent particles, while the majority of Mn content exists in solid solution, leading to a supersaturation of the solid solution. The supersaturated Mn will precipitate as Mn-bearing dispersoids during subsequent thermo-mechanical processing steps [2, 3]. As compared to the commonly occurring cube texture in the recrystallized direct chill (DC) cast Al alloys, annealing of deformed, supersaturated AA3xxx series aluminium alloys usually results in different recrystallization textures. The particles may affect the recrystallization texture in different ways. Coarse pre-existing constituent particles favour Particle

✉ K. Huang
huangke0729@hotmail.com

Y. J. Li
yanjun.li@ntnu.no

K. Marthinsen
knut.marthinsen@ntnu.no

¹ Department of Materials Science and Engineering,
Norwegian University of Science and Technology,
7491 Trondheim, Norway

² Thermomechanical Metallurgy Laboratory – PX Group
Chair, Ecole Polytechnique Fédérale de Lausanne (EPFL),
2002 Neuchâtel, Switzerland

Stimulated Nucleation (PSN) associated with a wide range of nucleus orientations, and thus normally yields an overall random recrystallization texture [4, 5]. Nevertheless, recent studies have shown that specific PSN texture components can still be developed during annealing due to the presence of these orientations after deformation within the deformation zone near the large particles [6–12]. More distinct textures may appear when the deformation is small [1], or at low recrystallization temperatures [13, 14]. On the other hand, fine dispersoids especially those precipitated during annealing (concurrent precipitation) may pin boundaries leading to a coarse, elongated grain structure [15] together with the P and ND-rotated cube texture components [7].

It has been reported [6–12, 16, 17] that P-oriented (sub-)grains already exist around the large particles after deformation. The evolution of the P-orientation as a function of precipitation in an AA3103 alloy was analysed by Sjølstad et al. [18], and a strong P-texture component was found when precipitation occurred simultaneously with recrystallization. Large grains with P and ND-rotated orientations were found to grow faster than randomly oriented grains, supposedly due to the fact that randomly oriented grains (also produced by PSN) are more sensitive to precipitation [7, 19]. In general, the P-texture has been observed after isothermal annealing of cold-rolled Al–Mn alloys with a highly supersaturated solid solution [7, 20, 21], large cold-rolling deformations [7, 22] and low annealing temperatures [7, 23]. Heating rate also plays a role, where the recrystallization texture can be characterized by a relatively strong P-texture and a $\sim 22.5^\circ$ ND-rotated cube orientation at low heating rates, while a weak cube texture was observed when rapid annealing is applied to the hot band of a continuous cast AA3105 aluminium alloy [24]. Bampton et al. [25] claimed that the coarse, elongated recrystallized grains obtained at low heating rates are mainly due to early activation of the most highly favoured nucleation sites (i.e. a nucleation preference), however, recrystallization textures were not addressed. Recent work however [12], following the microstructural evolution during non-isothermal annealing of a cold-rolled Al–Mn–Fe–Si alloy, showed no indications of a nucleation preference for the P-oriented grains. In this work [12], grain structures dominated by large elongated P-oriented grains were mainly observed for certain conditions where annealing was strongly influenced by dispersoids (pre-existing and/or formed by concurrent precipitation).

It has recently been shown that even starting from the same material, however, with different microchemistries, i.e. in terms of solutes and second-phase particles, may lead to distinctively different recrystallization microstructures and textures during non-isothermal annealing of a cold-rolled Al–Mn–Fe–Si alloy [12, 26]. Conclusions related to the factors affecting the P-texture, based on the

analysis of one alloy, may be contradictory to those obtained from another alloy, due to differences in microchemistry [12]. It may be concluded that, although extensively studied, the mechanisms and conditions for the formation and evolution of these coarse-grained structures dominated by a strong P-texture are in general still neither well understood nor well documented. As these P-oriented coarse, elongated grains may affect mechanical properties and anisotropy, a careful analysis of factors affecting the strength of the P-texture component is also important from a technological perspective.

Based on previous related studies [12, 20], an Al–Mn–Fe–Si alloy was homogenized at different conditions to give three different microchemistry states. The microchemistry state which is found to promote a pronounced P-texture after annealing was then used as the reference case in this study, and factors influencing the strength of the P-texture were analysed with respect to this variant. The main objective of the present work has been to systematically investigate important factors that influence the formation and the strength of the P-texture and to identify the conditions that promote a strong P-texture during recrystallization of a supersaturated Al–Mn–Fe–Si alloy. The microstructure and texture have been characterized by EBSD, which allow us to access not only the texture intensity, but also the size and number fraction of P-oriented grains that are not available with XRD analysis alone.

Experimental

The investigated material was a DC-cast AA3xxx extrusion billet of 288 mm in diameter, supplied by Hydro Aluminium, from which slabs were machined from the central region. The as-received material was in the as-cast state, with the chemical composition (wt%) of 0.152 % Si, 0.530 % Fe, 0.390 % Mn with the balance of Al. A detailed description of the as-cast material can be found in Ref [20].

The material and microstructure characterization details have been presented elsewhere [20], but key information will be reiterated here to increase the readability. The received as-cast material was homogenized at two different conditions to get different microchemistry. The homogenization treatment was performed in an air circulation furnace with a temperature accuracy of $\pm 2^\circ\text{C}$, starting from room temperature (about 20°C). To be consistent with previous work on the same set of alloys [12, 20, 21, 26], one set of samples in as-cast condition (C1-0) was heated at a heating rate of 50°C/h to 450°C and kept for 4 h, referred to as C1-2. Another set of samples was subjected to a two-stage homogenization treatment. The samples were first heated at 50°C/h to 600°C and held for

4 h, and then cooled at 25 °C/h to 500 °C where they were kept for another 4 h, which gave the condition denoted C1-3. The different homogenization procedures are summarized in Table 1.

The microchemistry characteristics of the as-cast condition (C1-0) as well as the two homogenized variants are listed in Table 2. It is noted that size distributions of constituent particles are similar for all these conditions, i.e. the potential for PSN is comparable in the three conditions. With respect to dispersoids, the C1-2 condition already contains a fairly high density of small dispersoids after homogenization. Previous studies have shown that this homogenization treatment promotes a sharp P recrystallization texture, especially at a low heating rate after cold rolling [12, 26]. The C1-3 and C1-0 variants, which both have a microchemistry distinctively different from C1-2, with C1-3 having both a fairly low concentration of Mn in solid solution (limited potential for concurrent precipitation) and a coarse dispersoid structure, were selected for comparison, to analyse the effect of microchemistry on the P-texture strength. Materials were water quenched to room temperature at the end of the homogenization procedure. The samples of all the three variants were cold rolled at room temperature in multiple passes to true strain of $\varepsilon = 1.6$ or $\varepsilon = 3.0$. The rolled sheets were then either isothermally annealed in a pre-heated salt bath or non-isothermally annealed in an air circulation furnace to the target temperature, and they were then held for 10^5 s at that temperature before water quench. The long holding time of 10^5 s was chosen to make sure that a fully recrystallized state was reached for all the investigated conditions, since recrystallization is rather slow at low annealing temperatures [20]. All the thermo-mechanical processing conditions used in this study are summarized in Table 1. Here, the C1-2 sample deformed to $\varepsilon = 3.0$, and then heated at 50 °C/h to 400 °C and held at this temperature for 10^5 s is taken as the reference case. Important factors like the microchemistry state, the cold deformation, the heating rate, as well as the target temperature were then changed systematically relative to the reference case. Unless specifically stated, the studied material is C1-2, the cold deformation before annealing is $\varepsilon = 3.0$ and the heating rate during non-isothermal annealing is 50 °C/h.

The crystallographic textures of the sheets were measured by means of Electron backscatter diffraction (EBSD) on a Zeiss Supra/Ultra 55 scanning electron microscope (SEM) equipped with TSL software. EBSD maps of the annealed samples, covering more than one thousand grains (except for the cases with extremely large grains), with a step size of 1–2 μm , were used to study the orientation of the recrystallized grains and thus the texture evolution during recrystallization. All SEM/EBSD micrographs were taken in the RD–ND plane and are presented such that the

RD is horizontal, and the ND is vertical. The grain size was measured as the equivalent circle diameter in the RD–ND cross section. The texture was represented in terms of orientation distribution functions (ODFs) using TSL OIM Analysis 6 software package by imposing orthotropic (rolling) sample symmetry, and using the harmonic series expansion method ($L = 22$) with a Gaussian half-width of 5° [27]. Since the focus of the recrystallization texture investigations in the present study is the $P\{011\}\langle 566 \rangle$ -texture component, which is located in the ODF section with $\varphi_2 = 0$, only this section is presented for each condition. Examples of typical full ODF maps can be found in [26]. This simplification might bring some ambiguity, since identical intensity of the P-texture component does not ensure the same volume fraction when the ODF max values at different conditions are not the same. So the area fraction of P-oriented grains obtained by EBSD is also provided for each condition, where all grains observed with an orientation within a 15° scatter (in all directions) from the ideal P-texture component are classified as belonging to this specific component.

Results

Effect of homogenization and microchemistry

The presence and intensity of the P-texture component is primarily determined by the microchemistry, which for the particular alloy studied in this work is determined by the homogenization procedure (Table 2). After isothermal annealing at 400 °C for 10^5 s, the strength of the P-texture component (see Fig. 1) in sample C1-3 is lower than that in sample C1-0, namely with decreasing amount of Mn in solid solution (see Table 2), and is barely visible for the C1-3 condition which exhibits a characteristic cube texture. Statistically, the area fractions and intensities of the P-component also decrease with the decreasing amount of Mn in solid solution, as listed in Table 3. The intensity of the P-texture correlates with the recrystallized grain size, which increases with the P-texture intensity (the corresponding recrystallized grain structures and their average grain size have been presented previously [20]). In general, the strength of the P-texture component during isothermal annealing are relatively weak.

In the case of non-isothermal annealing (heating the samples at 50 °C/h to 400 °C and then holding for 10^5 s) of the three variants, the strength of the P-texture in terms of ODF intensity and area fraction is generally stronger and the dependency on microchemistry is distinctively different, as shown in Fig. 2 and Table 3. The weakest P-texture intensity was obtained for C1-3, $\sim 5.7\times$ random, significantly higher than for isothermal annealing, but still

Table 1 Thermo-mechanical processing of the investigated samples by changing microchemistry, cold deformation, heating rate and annealing temperature

Material condition	Cold rolling (true strain)	Heating rate (°C/h)	Target temperature (with holding time of 10^5 s) (°C)			
C1-0	3.0	50	–	350	400	–
as-cast, no homogenization		7.6×10^6	–	–	400	–
C1-2	1.6	50	–	–	400	–
50 °C/h up to 450 °C/4 h		7.6×10^6	–	–	400	–
	3.0	50	325	350	400	500
		100	–	–	400	–
		200	–	–	400	–
		7.6×10^6	325	350	400	500
C1-3	3.0	50	–	–	400	–
50 °C/h up to 600 °C/4 h, 25 °C/h down to 500 °C/4 h		7.6×10^6	–	–	400	–

Isothermal annealing in salt bath corresponding to heating rate of $\sim 7.6 \times 10^6$

much weaker than the other two cases due to a limited number of pre-existing dispersoids and less concurrent precipitation. However, somewhat surprisingly, a quite pronounced P-texture ($\sim 25 \times$ random), and by far the strongest, was in this case obtained for C1-2, which has a lower amount of Mn in solid solution as compared to C1-0 (P-intensity: $\sim 10 \times$ random). The recrystallization textures of C1-2 after annealing at different conditions were thus chosen for further investigations, of which the results will be presented in the following section.

Effect of deformation and annealing conditions

The recrystallized grain structures of samples of the C1-2 alloy isothermally annealed at different temperatures for 10^5 s are shown in Fig. 3. It is noted that the differences in microstructure in terms of grain morphology and average grain size are limited at higher temperatures of 400 and 500 °C, as can be seen in Fig. 3a, b. In both cases, a slightly elongated grain structure was observed, and the average grain sizes were similar as well (24 μm at 400 °C and 23 μm at 500 °C). However, below 400 °C, the grain structure changes significantly and quite coarse, elongated grains result at the lowest annealing temperature of 325 °C (Fig. 3a). A corresponding variation has been observed for the recrystallization kinetics of the same alloy [20], which becomes extremely slow at the lowest temperatures.

The corresponding recrystallization textures, i.e. after the same isothermal annealing temperatures, are presented in Fig. 4. The recrystallized textures can for all cases be characterized by the Cube, ND-rotated cube and P-texture components, even though their relative intensities vary, as illustrated in Fig. 4. The P-texture component is not the dominant one for all of the four cases, although it is present at all temperatures. As can be seen from Table 4, the area

fraction of the P-texture component, which at maximum are found to be 22.9, 11.6, 7.2 and 7.2 % for the samples annealed at 325, 350, 400 and 500 °C, respectively, decreases consistently with the increasing annealing temperature. The maximum ODF intensities of the P-texture component are also listed in Table 4.

The samples were also non-isothermally heated to the same temperatures as used during isothermal annealing, i.e. 325, 350, 400, 500 °C, with the heating rate of 50 °C/h, after which they were kept at these temperatures for 10^5 s. The resulting recrystallized microstructures and corresponding textures are shown in Figs. 5 and 6, respectively. Much coarser grain structures were obtained for all annealing conditions when the samples were non-isothermally annealed at different target temperatures (see Fig. 5), as compared to their isothermal counterparts annealed at the same temperatures (see Fig. 3).

As compared to the isothermal cases, the most striking difference in terms of recrystallization texture for the non-isothermal cases is related to the P-texture component, as shown in Fig. 6. In addition to being the most dominant texture component for all conditions after non-isothermal annealing (as listed in Table 4), its intensity and area fraction were significantly higher than its counterpart after isothermal annealing, clearly demonstrating that non-isothermal annealing promotes a stronger P-texture. It is worth to notice that the intensity and area fraction of the P-texture component vary with temperature non-monotonically, they first decrease and then increase again when increasing the annealing temperature from 325 to 500 °C. This will be addressed in more detail in “Discussion” section, below.

The effect of cold deformation (amount of rolling strain) prior to annealing on the intensity of the P-texture was also analysed for the C1-2 samples, both using isothermal as

Table 2 Electrical conductivity, concentrations of solutes, average diameter and number density of particles in the alloys studied [12]

	Electrical conductivity (m/Ωmm ²)	Concentration of Mn (wt%)	Constituent particles		Dispersoids	
			Average Diameter (μm)	Number density (mm ⁻²)	Average Diameter (μm)	Number density (mm ⁻²)
C1-0	23.9	0.35	0.88	2.8e4	–	–
C1-2	27.5	0.16	0.96	2.9e4	0.054	1.3e6
C1-3	29.0	0.11	1.10	2.1e4	0.127	5.5e4

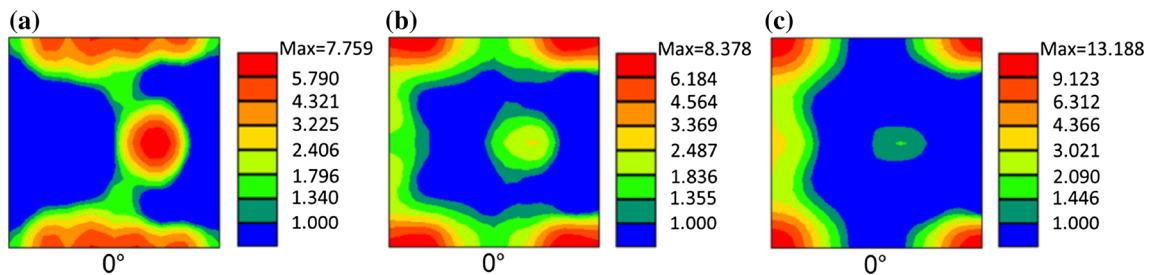


Fig. 1 ODF maps ($\varphi_2 = 0$) showing the recrystallization texture after isothermal annealing with different microchemistry states at 400 °C for 10⁵ s, the samples were previously cold rolled to $\epsilon = 3.0$. **a** C1-0; **b** C1-2; **c** C1-3

Table 3 Statistics of P-texture components after isothermal annealing and non-isothermal annealing (50 °C/h) to 400 °C and holding for 10⁵ s for the three variants, the samples were previously cold rolled to $\epsilon = 3.0$

	C1-0	C1-2	C1-3
Isothermal annealing			
ODF intensity ($f(g)$)	7.7	2.6	1.5
Area fraction (%)	16.3	7.2	3.5
Number fraction (%)	7.5	5.8	3.3
Non-isothermal annealing			
ODF intensity ($f(g)$)	10.2	24.7	5.7
Area fraction (%)	20.8	46.2	12.3
Number fraction (%)	15.3	20.8	7.7

well as non-isothermal heating and annealing. As shown in Fig. 7 and Table 5, a weaker P-texture component (2 × random, with area fraction of 6.6 %) was found at a smaller cold deformation corresponding to a rolling strain of $\epsilon = 1.6$, as compared to the sample deformed to the larger strain of $\epsilon = 3.0$ (2.6 × random, with area fraction of 7.2 %) with subsequent isothermal annealing (see Fig. 4c). The decrease of strength of the P-texture with smaller cold deformations is more evident after non-isothermal annealing, see Figs. 6c and 7b, which is also accompanied by the presence of a quite distinct ND-rotated cube component. The area fractions of P-oriented grains decreased from 46.2 to 16.0 % when the cold deformation was decreased from 3.0 to 1.6, as listed in Table 5.

Finally, the influence of heating rate during non-isothermal annealing to the target temperature was investigated. Four samples were annealed at different heating rates up to 400 °C and were then kept at this temperature for 10⁵ s. The four heating rates were 50, 100, 200 and 7.6×10^6 °C/h (where the latter one corresponds to isothermal annealing, which also can be considered as ultra-fast non-isothermal annealing), respectively. The resulting textures (ODF-maps, $\varphi_2 = 0$ section) are presented in Fig. 8, and the corresponding P-texture intensities and area fractions are presented in Table 6. It is clear and consistent from Fig. 8 and Table 6 that a rapid heating rate weakens the strength of the P-texture. At lower heating rates (see Fig. 8a–c), the P-texture component is the dominant one. Cube and ND-rotated cube components become the major texture components at the highest heating rate, i.e. isothermal annealing, as illustrated in Fig. 8d.

Discussion

The results obtained, in terms of grain structures and the P-texture strength in particular, are discussed in this section in view of the influence of dispersoids, pre-existing and/or formed during annealing (concurrent precipitation) on the recrystallization behaviour. Dispersoids influence the recrystallization behaviour in several ways: (1) dispersoids may slow down and reduce the nucleation rate and may even completely suppress nucleation of recrystallization

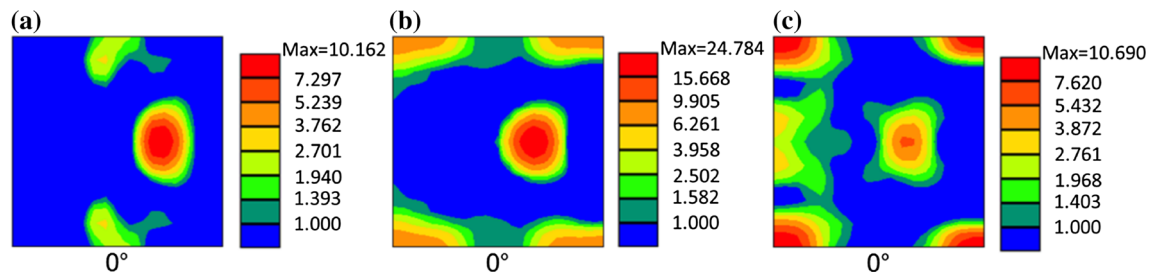
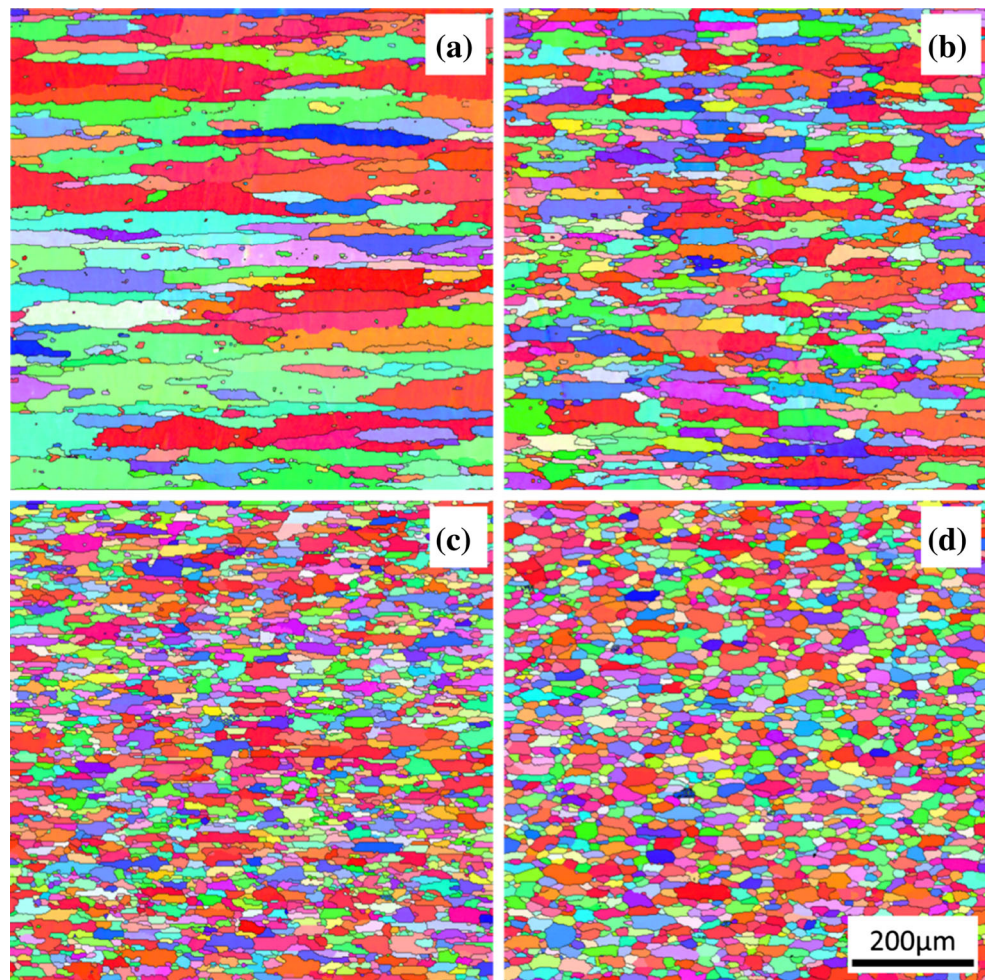


Fig. 2 ODF maps ($\varphi_2 = 0$) showing the recrystallization texture after non-isothermal annealing (50 °C/h) with different microchemistry states at 400 °C for 10^5 s, the samples were previously cold rolled to $\varepsilon = 3.0$. **a** C1-0; **b** C1-2; **c** C1-3

Fig. 3 EBSD micrographs showing the recrystallized grain structure of C1-2 samples after isothermal annealing at different temperatures for 10^5 s, the samples were previously cold rolled to $\varepsilon = 3.0$. **a** 325 °C, **b** 350 °C, **c** 400 °C, **d** 500 °C



through their influence (Zener pinning effect) on sub-grain (low-angle grain boundary) growth, i.e. the incubation time before onset of recrystallization increases; (2) dispersoids may impede grain boundary migration of a growing recrystallized grain (high-angle grain boundary), also through a Zener drag force, which slow down the overall recrystallization kinetics. Dispersoids can be precipitated mainly before, during or after recrystallization. Pre-existing dispersoids formed during homogenization will influence the recrystallization behaviour both during the

nucleation stage and during the growth stage, unless they are dissolved again into the matrix during annealing. The effect of concurrently precipitated dispersoids, if formed during the nucleation stage and mainly before recrystallization is completed, may be even stronger, due to their spatial distribution (mainly along sub-grain/grain boundaries) and often smaller size [28]. In principle, the precipitation reaction may also be influenced by the recrystallization process, through the gradual removal of heterogeneous nucleation sites and fast diffusion paths

Fig. 4 ODF maps ($\varphi_2 = 0$) showing the recrystallization texture of C1-2 samples after isothermal annealing at different temperatures for 10^5 s, the samples were previously cold rolled to $\varepsilon = 3.0$. **a** 325 °C, **b** 350 °C, **c** 400 °C, **d** 500 °C

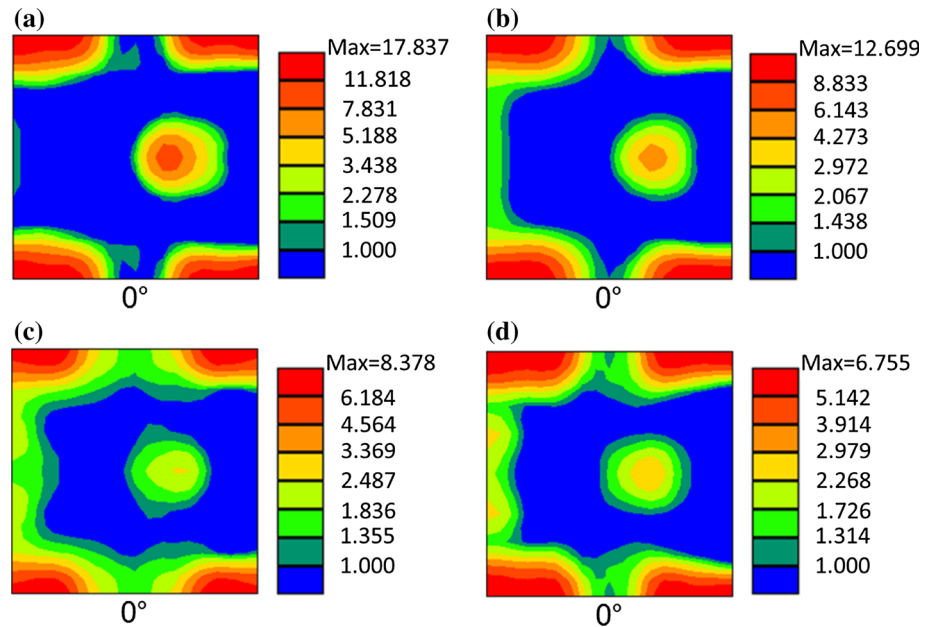


Table 4 ODF intensities and area fractions of P-texture components after isothermal and non-isothermal annealing (50 °C/h) for C1-2, the samples were previously cold rolled to $\varepsilon = 3.0$

Temperature (°C)	325	350	400	500
Isothermal annealing				
ODF intensity ($f(g)$)	9.3	5.1	2.6	2.6
Area fraction (%)	22.9	11.6	7.2	7.2
Non-isothermal annealing				
ODF intensity ($f(g)$)	31.9	20.2	24.7	38.8
Area fraction (%)	45.7	41.8	46.2	51.8

(dislocations). However, this is in the present context believed to be a second-order effect and will not be discussed in this work.

The C1-2 condition contains a considerable amount of pre-existing dispersoids and their effect on the recrystallized grain structure at different (isothermal) annealing temperatures is illustrated in Fig. 3. As observed, the influence is significantly different at different temperatures. At high temperatures (note the small difference between annealing at 400 and 500 °C), recrystallization completes generally fast, and the pre-existing dispersoids seem to have a small influence on both kinetics and the recrystallized grain structure (as compared to conditions mainly without dispersoids [20]). At lower annealing temperatures (Fig. 3a, b; still only another drop of 50 and 75 °C, respectively), on the contrary, the influence of the pre-existing dispersoids seems much stronger giving much coarser grain structures, especially at 325 °C, where also the kinetics has been found to be extremely slow [20]. Since both nucleation and growth of recrystallization are

thermally activated processes, parts of the changes may be attributed to temperature alone and possibly additional concurrent precipitation (most pronounced at the lowest temperature). However, the effects at the lowest annealing temperature are far too strong, and our previous work have shown that annealing the same alloy mainly without dispersoids (C1-3) at 300 °C gives a fairly fined grain material [20], clearly showing that this is mainly the effect of dispersoids. The fact that the grain size increases so much also illustrates that the influence is mainly on the nucleation behaviour, by strongly reducing the nucleation rate. The strongly elongated grains, however, is a growth effect due to a stronger Zener drag in the ND direction than the RD direction (see Ref. [12] and further discussion below).

A similar trend with temperature has also been observed in conditions where concurrent precipitation dominates, e.g. with the as-cast variant (C1-0) [20], however, where the variations with temperature may be even stronger. In this case, at the highest temperatures, recrystallization completes very fast, before any significant concurrent precipitation takes place, and any influence is mainly avoided. At lower temperatures, precipitation kinetics is faster, while recrystallization becomes slower and the influence becomes significant. Finer and heterogeneously distributed dispersoids (along boundaries) may strengthen the effects [28].

Turning to the presence and strength of the P-texture component it is well documented that it is closely related to the presence of dispersoids, and concurrent precipitation in particular (e.g. [7, 12, 20, 26, 28]). It is further assumed to be intimately connected with particle stimulated nucleation of recrystallization. Recent studies by EBSD, TEM and finite

Fig. 5 EBSD micrographs showing the recrystallized grain structure after non-isothermal of C1-2 samples, the samples were previously cold rolled to $\varepsilon = 3.0$ and then heated at $50\text{ }^\circ\text{C/h}$ to the different target temperatures and held for 10^5 s . **a** $325\text{ }^\circ\text{C}$, **b** $350\text{ }^\circ\text{C}$, **c** $400\text{ }^\circ\text{C}$, **d** $500\text{ }^\circ\text{C}$

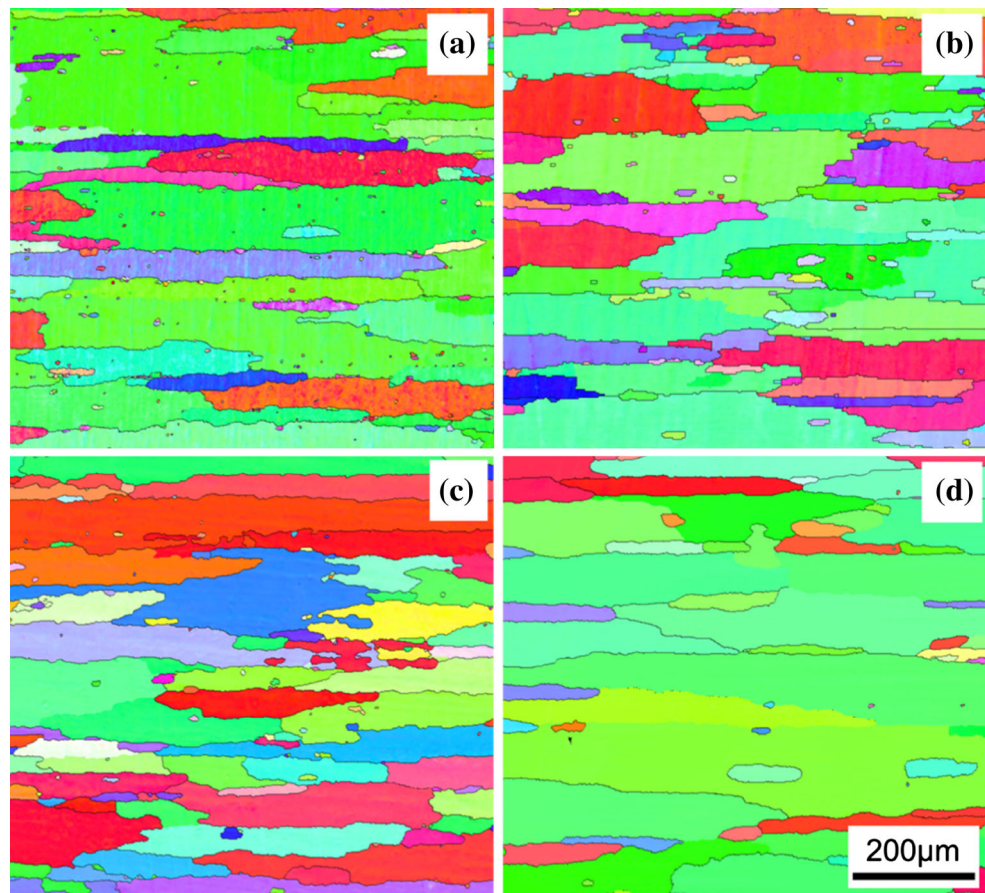
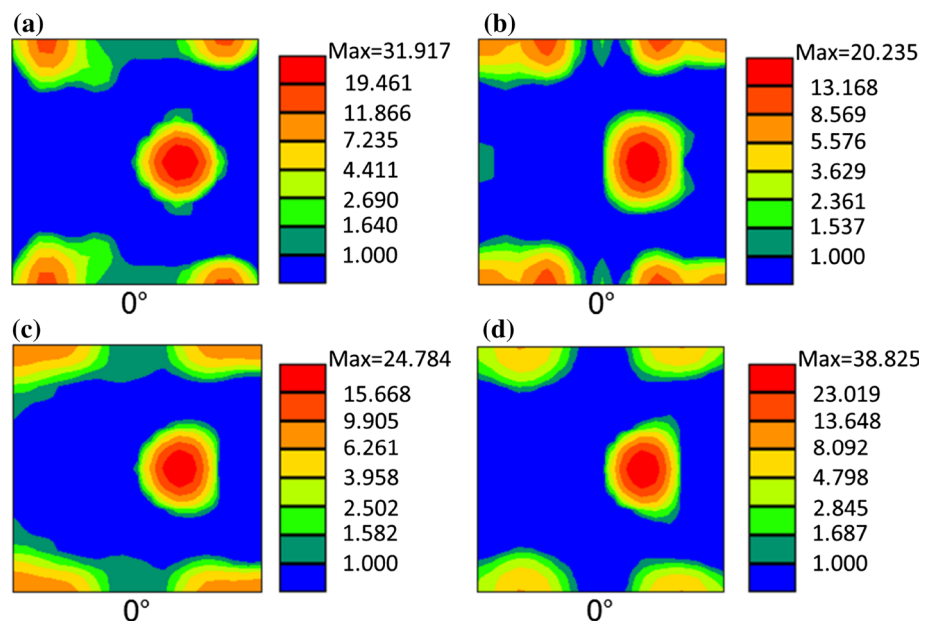


Fig. 6 ODF maps ($\varphi_2 = 0$) showing the recrystallization texture after non-isothermal annealing of C1-2 samples, the samples were previously cold rolled to $\varepsilon = 3.0$ and then heated at $50\text{ }^\circ\text{C/h}$ to the different target temperatures and held for 10^5 s . **a** $325\text{ }^\circ\text{C}$, **b** $350\text{ }^\circ\text{C}$, **c** $400\text{ }^\circ\text{C}$, **d** $500\text{ }^\circ\text{C}$



element method demonstrated that P-oriented grains/subgrains already exist within the deformation zone around constituent particles after deformation [6–12, 16, 17]. The microstructure evolution during non-isothermal annealing

of the *same material* was investigated in detail in Ref [12], where it was demonstrated that P-oriented grains indeed can be found near particles, but they can be also observed in the deformed matrix away from the deformation zone.

Fig. 7 ODF maps ($\varphi_2 = 0$) showing the recrystallization texture of C1-2 samples at 400 °C for 10⁵ s, the samples were previously cold rolled to $\varepsilon = 1.6$. **a** Isothermal annealing, **b** non-isothermal annealing

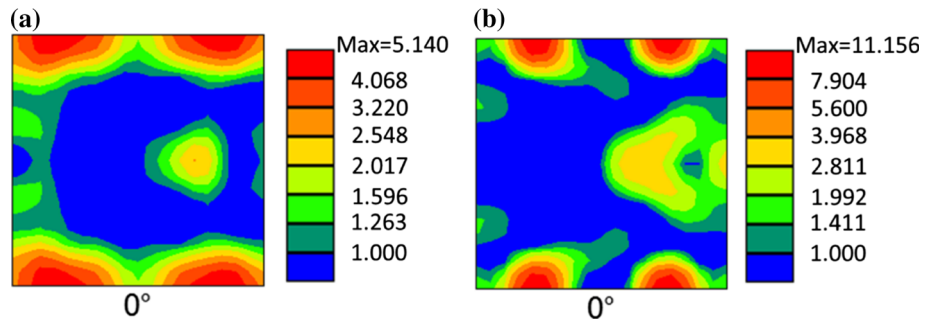


Table 5 Statistics of P-oriented grains, samples were deformed to $\varepsilon = 1.6$ before isothermal or non-isothermal annealing at 400 °C for 10⁵ s

	ODF intensity ($f(g)$)	Area fraction (%)	P-grain size (μm)	Number fraction (%)	Grain size (μm)
Isothermal annealing	2.0	6.6	29	5.3	28
Non-isothermal annealing	3.5	16.0	120	7.7	106

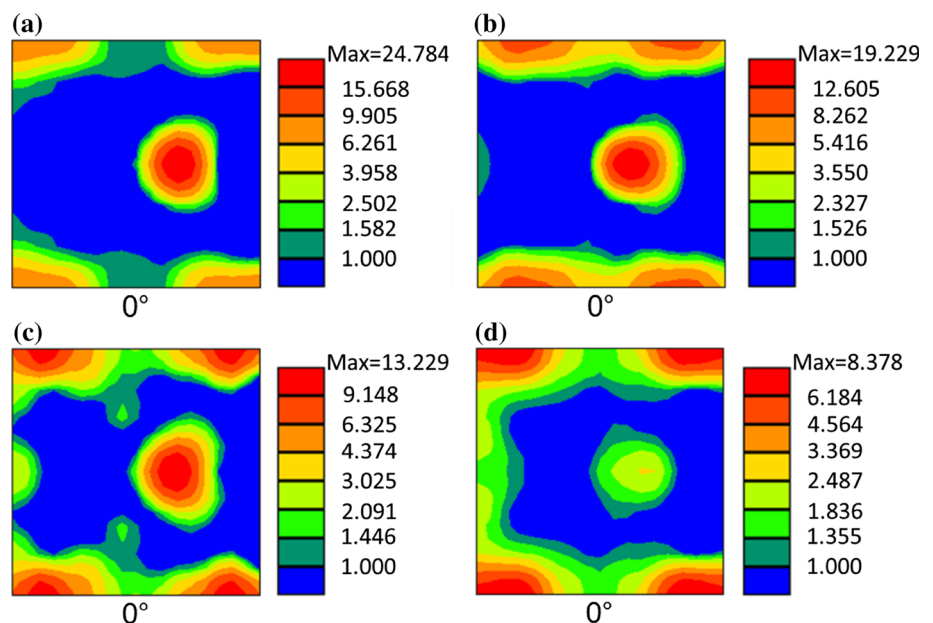
Table 6 Statistics of P-oriented grains heating at different heating rates to 400 °C and holding for 10⁵ s for C1-2, the samples were previously cold rolled to $\varepsilon = 3.0$

Heating rate (°C/h)	50	100	200	7.6×10^6
ODF intensity ($f(g)$)	24.7	19.2	13.2	2.6
Area fraction (%)	46.2	32.0	29.3	7.2
Number fraction	20.8	15.9	15.2	5.8

The very strong P-texture observed in the present work, during non-isothermal annealing at low temperatures of the C1-2 variant, was further analysed by plotting the average grain size of all the grains and the P-oriented grains, as

illustrated in Fig. 9. The average grain sizes after non-isothermal annealing were significantly larger than those after isothermal annealing at the same (holding) temperatures. The main difference between isothermal and non-isothermal annealing lies in the concurrently precipitated dispersoids, recovery and even recrystallization during the heating stage of non-isothermal annealing, which all strongly influence the recrystallization behaviour and the final recrystallized structure. Changes of the constituent particle structures during the heating stage are small, especially at temperatures below 400 °C, and are thus not expected to play any role. P-oriented grains clearly have a growth/size advantage over grains with other

Fig. 8 ODF maps ($\varphi_2 = 0$) showing the recrystallization texture after non-isothermal annealing of C1-2 samples with different heating rates at 400 °C for 10⁵ s, the samples were previously cold rolled to $\varepsilon = 3.0$. **a** 50 °C/h, **b** 100 °C/h, **c** 200 °C/h, **d** isothermal annealing



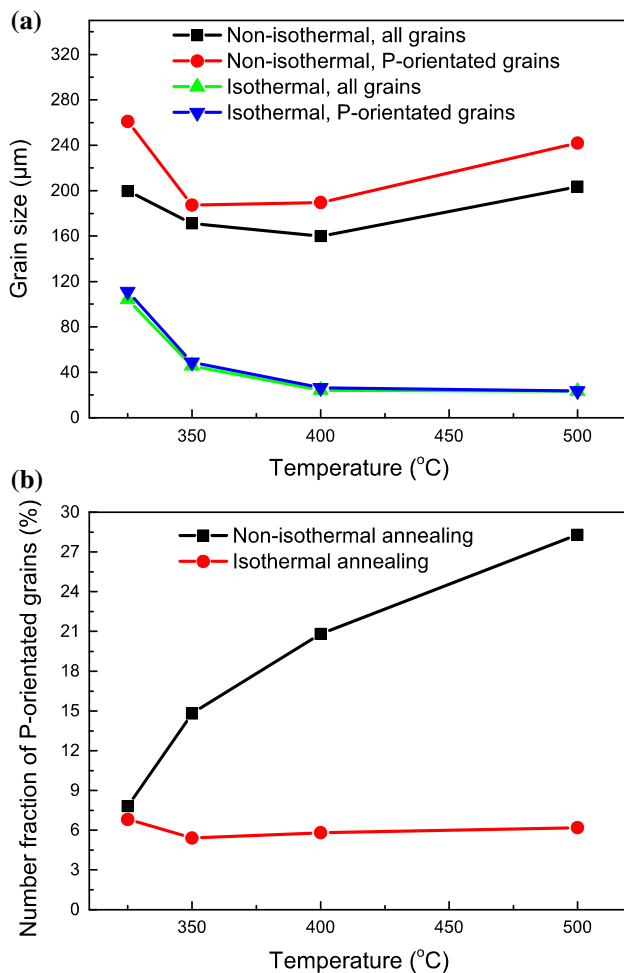


Fig. 9 The variation of grain size and number fraction of P-oriented grains after isothermal and non-isothermal annealing (50 °C/h) of C1-2 samples at 400 °C for 10^5 s, the samples were previously cold rolled to $\varepsilon = 3.0$. **a** The average grain sizes, **b** number fraction of P-oriented grains

orientations for non-isothermal annealing, especially at the lowest annealing temperature, an effect which is mainly absent for isothermal annealing. During non-isothermal annealing, concurrently precipitated dispersoids form at lower temperatures and affect the recrystallization behaviour at higher temperatures [12]. P-oriented grains experience a growth advantage at lower temperatures, since these grains are assumed to be less affected by dispersoids [7, 12]. With the heating rate of 50 °C/h, recrystallization is completed when reaching to 350 °C [12], which implies that mainly grain growth is responsible for both the evolution of grain size and recrystallization texture at target temperatures higher than 350 °C. The sharp P-texture obtained after non-isothermal annealing at 325 °C for C1-2 (see Fig. 6a) is obviously due to the growth/size advantage of the P-oriented grains (Fig. 9a), since their number fraction is the smallest among the four conditions with

different temperatures as shown in Fig. 9b. The fact that the number fraction of P-oriented grains increases above 350 °C indicates that P-oriented grains must have consumed recrystallized grains with other orientations during the grain growth stage. This also explains why the strength of the P-texture component increased after non-isothermal annealing at temperatures above 400 °C (Fig. 6 and Table 4) where the growth advantage did not increase (see Fig. 9a).

The grain growth at high temperatures observed after non-isothermal annealing in the present work may be due to the increased grain boundary mobility at higher temperature. Second-phase particles (dispersoids) formed at lower temperatures might also have played a role, since they can either coarsen or even dissolve at higher temperatures and thus reduce their dragging effect on grain boundary migration. This assumption is supported by the decrease of electrical conductivity during non-isothermal annealing of C1-2 at temperatures larger than 400 °C reported previously [12]. During isothermal annealing, especially at temperatures larger than 350 °C, recrystallization completes very fast [20] and the influence of concurrent precipitation and recrystallization is mostly avoided, so P-oriented grains do not exhibit any size advantage after recrystallization, neither do they have any nucleation advantage (see Fig. 9b).

When the cold deformation decreased from $\varepsilon = 3.0$ to $\varepsilon = 1.6$, the area fraction of the P-texture component after non-isothermal annealing at 400 °C rapidly decreased from 46.2 % random to 16.0 %, as shown in Tables 4 and 5. With smaller cold deformation and thus less stored energy (i.e. driving force for recrystallization), the onset of recrystallization takes place at higher temperatures, where the growth advantage of P-oriented grains is less, which then leads to a weaker P-texture. Limited change was observed after isothermal annealing due to the already weak P-textures. This latter observation seems to suggest that large deformation promotes stronger P-texture only when the influence of second-phase particles (dispersoids) on recrystallization is significant. It should be mentioned, though, that a pronounced P-texture was also reported [29] after isothermal annealing of commercially pure AA1050 alloy, which has limited number of particles, deformed to ultrahigh strains. Ultrahigh strains may lead to a very small critical particle size for PSN, consistent with the fact that PSN generally occurs above a critical particle size which decreases with increasing strain [30]. When decreasing the cold deformation in the present work from 3.0 to 1.6, the number fraction of P-oriented grains decreased slightly after isothermal annealing (5.8 and 5.3 % respectively). However, after non-isothermal annealing, the number fraction decreased significantly more, from 20.8 to 7.7 %.

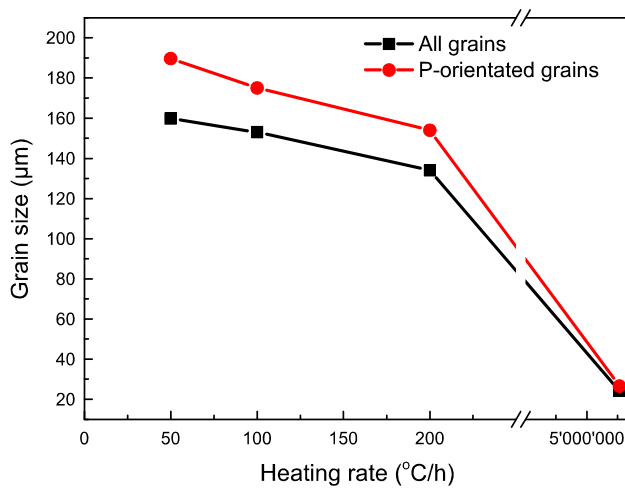


Fig. 10 The variation of grain sizes of C1-2 samples annealed at 400 °C for 10^5 s with different heating rates, the samples were previously cold rolled to $\varepsilon = 3.0$

The effect of heating rate on recrystallized grain size has been extensively analysed [25, 31–33], however, the corresponding possible influence on recrystallization textures has been given less attention [34]. Liu et al. [24] studied the effect of heating rate on the microstructure and texture of a continuous cast AA3105 aluminium alloy with two different heating rates, i.e. 660 °C/h and 1.8×10^5 °C/h, respectively. Compared to the present work, different annealing temperatures and holding times were used in their study, and cases at even lower heating rates were left unexploited. The reason why a highly elongated grain structure is obtained during non-isothermal annealing of the alloy investigated in the present work has been discussed in detail in another paper [12]. For cold-rolled Al–Mn(–Fe–Si) alloys at low annealing temperatures, the supersaturated Mn in solid solution precipitate on the grain/sub-grain boundaries, which are aligned with the RD direction. These dispersoids strongly suppress nucleation of recrystallization and also provide a stronger Zener drag effect in the ND direction than along RD, and thus an elongated grain structure results [12, 15]. The variation of the average recrystallized grain size of all grains and P-oriented grains only, with heating rate, is shown in Fig. 10. It can be seen that the average grain size both for all grains and the P-oriented grains are sensitive to the heating rate, where both the size/growth advantage and average grain size decrease with increasing heating rate. As compared to isothermal annealing, recovery and precipitation take place during the heating stage for non-isothermal annealing, both of which become more evident at lower heating rates and thus finally lead to larger average grain sizes. Evidence of considerable recovery and precipitation when heating the samples at 50 °C/h to 300 °C can be found in [12] in terms of hardness and electrical

conductivity evolution, as well as backscattered electrons (BSE) images.

Unlike isothermal annealing, where the effect of concurrent precipitation can be avoided at high temperatures since recrystallization kinetics is relatively fast, the dispersoids precipitated at lower temperatures will affect the softening behaviour at higher temperatures during non-isothermal annealing [12]. Somerday and Humphreys [15] found that at high heating rates precipitation mainly occurred at high-angle grain boundaries (HAGBs), whereas for low heating rates also medium-angle grain boundaries experienced precipitation. In the latter case, nucleation sites other than at particles, e.g. at grain boundaries are largely suppressed, which further promotes the preferential growth of the P-grains (exist near particles after deformation) at low heating rates owing to the hindered nucleation at other sites [8]. With lower heating rates, growth advantage prevails for a longer time and influences the recrystallization behaviour more strongly. For isothermal annealing, Tangen et al. [7] reported that dispersoids initially precipitated preferentially on HAGBs, while more homogeneously distributed dispersoids were observed on all boundaries with varying boundary misorientations for longer annealing times. At the lowest heating rate (50 °C/h), both HAGBs and low-angle grain boundaries (LAGBs) are supposed to experience concurrent precipitation. So, a large number fraction of P-oriented grains (see Table 6), which are less affected by concurrent precipitation, are obtained. These P-oriented grains also experience a size/growth advantage as compared to other grains, as shown in Fig. 10. This leads to a sharp P-texture after recrystallization. Increasing the heating rate reduces the time period for which P-oriented grains have a growth advantage as being less affected by concurrent precipitation, and finally a fairly weak P-texture results, as illustrated in Fig. 8 and Table 6.

The microchemistry state affects the strength of the P-texture component in two different ways, as illustrated in Table 3 and Fig. 11. During isothermal annealing at 400 °C, the intensities of the P-texture component were relatively weak due to (i) relatively fast recrystallization kinetics and generally small influence from dispersoids, and (ii) no or limited nucleation/growth advantage for P-oriented grains, i.e. all nucleation mechanisms are active at this temperature. The P-texture intensities and area fraction decrease with the amount of Mn in solid solution (prior to annealing), i.e. from sample C1-0 to sample C1-3. The as-cast variant, which possesses the highest Mn content in solid solution (see Table 2), and thus also most concurrent precipitation, obviously provides the strongest growth advantage (Fig. 11) and the largest number fraction of P-oriented grains (Table 3) after *isothermal* annealing. This is also consistent with the results presented in the

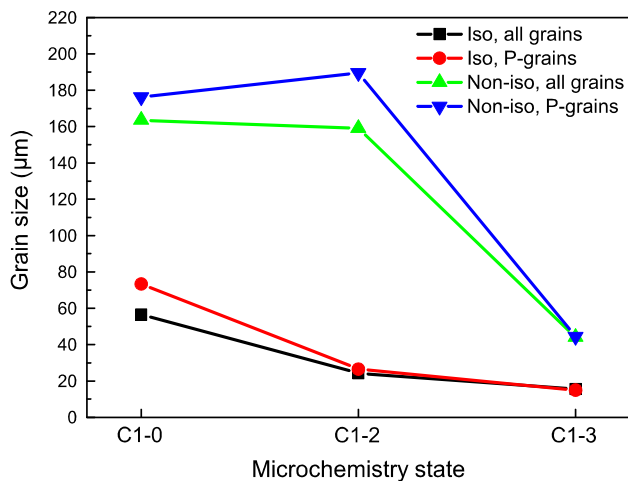


Fig. 11 The variation of grain sizes of samples annealed after isothermal and non-isothermal annealing (50 °C/h) at 400 °C for 10^5 s with different microchemistry states, the samples were previously cold rolled to $\varepsilon = 3.0$

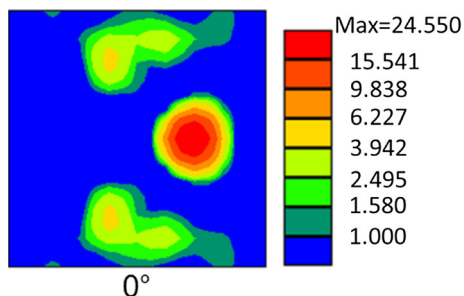


Fig. 12 ODF maps ($\varphi_2 = 0$) showing the recrystallization texture after non-isothermal annealing (50 °C/h) for C1-0 at 350 °C for 10^5 s, the samples were previously cold rolled to $\varepsilon = 3.0$

work by Tangen et al. [7] in the sense that the strength of P-texture component increases with the content of Mn in solid solution during isothermal annealing of similar alloys. However, although the C1-0 condition provides the strongest concurrent precipitation, the sharpest P-texture was still (perhaps somewhat unexpectedly) observed for C1-2 after *non-isothermal* annealing, as shown in Table 3. This was explained in detail in [12], where it was found that recrystallization started at a lower temperature for C1-2 as compared to C1-0 (even though the target temperature is the same, i.e. 400 °C, recrystallization started at different temperatures for C1-2 and C1-0 due to their different microchemistries), where the growth advantage of P-oriented grains is promoted for C1-2. This interpretation is supported by the fact that when C1-0 was non-isothermally annealed at the lower temperature of 350 °C (see Fig. 12), a sharper P-texture was actually obtained for this condition ($24.5\times$ random), as compared to that $20.2\times$ random for

C1-2 subjected to the same annealing condition as shown in Fig. 6b and Table 4.

Conclusions

A number of key factors affecting the presence and strength of the P{011} \langle 566 \rangle -texture component after annealing of a cold-rolled Al–Mn–Fe–Si alloy, relating to material microchemistry (solid solution level and dispersoids) and processing conditions during deformation and subsequent annealing, have been systematically investigated. The strength of the P-texture component was analysed in terms of ODFs, grain size and number fraction at different conditions using Electron Back Scattering Diffraction (EBSD). The presence and strength of the P-texture component is intimately related to dispersoids (whether pre-existing or as result of concurrent precipitation), and the results are thus discussed in view of how and to which extent these dispersoids influence the recrystallization nucleation and growth behaviour in different conditions. The main findings may be summarized as follows:

- (1) It was found that decreasing annealing temperature and heating rate, as well as increasing the amount of deformation before annealing, promotes a stronger P-texture, and these effects are more evident when the dominant texture is the P-component.
- (2) The microchemistry (in terms of pre-existing dispersoids and/or potential for concurrent precipitation) affects the strength of P-texture differently depending on the heating rate. With fast heating rate or isothermal annealing, the strongest P-texture component was observed when the initial amount of Mn in solid solution is the highest (largest potential for concurrent precipitation).
- (3) A sharpening of the P-texture can be found when the heating rate is reduced. The intensity of the P-texture was also significantly affected by the temperature at which recrystallization occurs.
- (4) Detailed analyses with EBSD clearly show that for conditions which favour a sharp P-texture component, P-oriented grains are larger than the average grain size at lower temperatures and these grains further grow at the expense of grains with other orientations at higher temperatures.

Acknowledgements This research work has been supported by the KMB Project (193179/140) in Norway. The financial support by the Research Council of Norway and the industrial partners, Hydro Aluminium and Sapa Technology, is gratefully acknowledged. KH acknowledges the financial support from Norwegian University of Science and Technology through Strategic Area Materials.

References

- Humphreys FJ, Hatherly M (2004) Recrystallization and related annealing phenomena, 2nd edn. Elsevier, Oxford
- Li YJ, Zhang WZ, Marthinsen K (2012) Precipitation crystallography of plate-shaped Al-6(Mn, Fe) dispersoids in AA5182 alloy. *Acta Mater* 60:5963–5974
- Li YJ, Arnberg L (2003) Quantitative study in the precipitation behavior of dispersoids in DC-cast AA3003 alloy during heating and homogenization. *Acta Mater* 51:3415–3428
- Lücke K, Engler O (1990) Effects of particles on development of microstructure and texture during rolling and recrystallisation in fcc alloys. *Mater Sci Technol* 6:1113–1130
- Vatne HE, Engler O, Nes E (1997) Influence of particles on recrystallisation textures and microstructures of aluminium alloy 3103. *Mater Sci Technol* 13:93–102
- Schäfer C, Gottstein G (2009) Modeling of texture evolution in the deformation zone of second-phase particles. *Acta Mater* 57:1026–1034
- Tangen S, Sjølstad K, Furu T, Nes E (2010) Effect of concurrent precipitation on recrystallization and evolution of the P-texture component in a commercial Al–Mn alloy. *Metall Mater Trans A* 41A:2970–2983
- Schäfer C, Gottstein G (2011) The origin and development of the P{011}<111> orientation during recrystallization of particle-containing alloys. *Int J Mater Res* 102:1106–1114
- Mishin OV, Godfrey A, Jull Jensen D, Hansen N (2013) Recovery and recrystallization in commercial purity aluminium cold rolled to an ultrahigh strain. *Acta Mater* 61:5354–5364
- Sidor JJ, Petrov RH, Kestens LAI (2014) Modeling the crystallographic change in processing of Al alloys. *J Mater Sci* 49:3529–3540. doi:10.1007/s10853-014-8068-8
- Sidor JJ, Decroos K, Petrov RH, Kestens LAI (2015) Evolution of recrystallization textures in particle containing Al alloys after various rolling reductions: Experimental study and modelling. *Int J Plasticity* 66:119–137
- Huang K, Engler O, Li YJ, Marthinsen K (2015) Evolution in microstructure and properties during non-isothermal annealing of a cold-rolled Al–Mn–Fe–Si alloy with different microchemistry states. *Mater Sci Eng A* 628:216–229
- Ørsund R, Nes E (1988) Effect of particles on recrystallization textures in aluminium–manganese alloys. *Scr Metall* 22:665–669
- Ørsund R, Nes E (1988) A model for the nucleation of recrystallization from particles: the texture aspect. *Scr Metall* 22:671–676
- Somerday M, Humphreys FJ (2003) Recrystallization behavior of supersaturated Al–Mn alloys. *Mater Sci Technol* 19:20–29
- Engler O (1996) Nucleation and growth during recrystallisation of aluminium alloys investigated by local texture analysis. *Mater Sci Tech* 12:859–872
- Ryu J-H, Lee DN (2002) The effect of precipitation on the evolution of recrystallization texture in AA8011 aluminum alloy sheet. *Mater Sci Eng A* 336:225–232
- Sjølstad K, Engler O, Tangen S, Marthinsen K, Nes E (2002) Recrystallization textures and the evolution of the P-orientation as a function of precipitation in an AA3103 alloy. *Mater Sci Forum* 408–412:1471–1476
- Daaland O, Nes E (1996) Recrystallization texture development in commercial Al–Mn–Mg alloys. *Acta Mater* 44:1413–1435
- Huang K, Wang N, Li YJ, Marthinsen K (2014) The influence of microchemistry on the softening behaviour of two cold-rolled Al–Mn–Fe–Si alloys. *Mater Sci Eng A* 601:86–96
- Huang K, Li YJ, Marthinsen K (2014) Isothermal annealing of a cold-rolled Al–Mn–Fe–Si alloy with different microchemistry states. *Trans Nonferrous Met Soc China* 24:3840–3847
- Liu WC, Morris JG (2006) Effect of hot and cold deformation on the P {011}<455>; recrystallization texture in a. *Scr Mater* 54:2095–2099
- Liu WC, Morris JG (2007) Recrystallization textures of the M{113}<110>; and P{011}<455>; orientations in a supersaturated Al–Mn alloy. *Scr Mater* 56:217–220
- Liu WC, Li Z, Man C-S (2008) Effect of heating rate on the microstructure and texture of continuous cast AA 3105 aluminum alloy. *Mater Sci Eng A* 47:173–180
- Bampton CC, Wert JA, Mahoney MW (1982) Heating rate effects on recrystallised grain size in two Al–Zn–Mg–Cu alloys. *Metall Mater Trans A* 13A:193–198
- Huang K, Zhao QL, Li YJ, Marthinsen K (2014) Non-isothermal annealing of a cold-rolled Al–Mn–Fe–Si alloy with different microchemistry states. *J Mater Process Technol* 221:87–99
- Engler O, Randle V (2010) Introduction to texture analysis: macrotexture, microtexture and orientation mapping, 2nd edn. CRC Press, Boca Raton
- Huang K, Li YJ, Marthinsen K (2015) Effect of heterogeneously distributed pre-existing dispersoids on the recrystallization behaviour of a cold-rolled Al–Mn–Fe–Si alloy. *Mater Charact* 102:92–97
- Mishin OV, Juul Jensen D, Hansen N (2010) Evolution of microstructure and texture during annealing of aluminium AA1050 cold rolled to high and ultrahigh strains. *Metall Mater Trans A* 41A:2936–2948
- Humphreys FJ (1977) The nucleation of recrystallization at second phase particles in deformed aluminium. *Acta Metall* 25:1323–1344
- Ferry M, Jones D (1997) High-rate annealing of single-phase and particle-containing aluminium alloys. *Scr Mater*. 38:177–183
- Sun N, Patterson BR, Suni JP et al (2008) Effect of heating rate on recrystallization of twin roll cast aluminum. *Metall Mater Trans A* 39:165–170
- Attallah MM, Strangwood M, Davis CL (2010) Influence of the heating rate on the initiation of primary recrystallization in a deformed Al–Mg alloy. *Scr Mater*. 63:371–374
- Huang K, Li YJ, Marthinsen K (2015) The influence of microchemistry on the recrystallization texture of cold-rolled Al–Mn–Fe–Si alloys. *IOP Conf Ser: Mater Sci Eng* 82:012035